Imaging sub-basalt structures using locally converted waves

Mirko van der Baan[1], Tom Kerrane[2], J-Michael Kendall[3], Neil Taylor[4]

Introduction

In many parts of the world large-scale basalt flows associated with continental rifting have blanketed pre-existing sedimentary basins. In recent years considerable attention has turned to exploration beneath these extensive flows. A region of particular interest is the Atlantic margin of northwest Europe which experienced early tertiary magmatism associated with the interaction of the Iceland plume and the opening of the Atlantic Ocean (Barton and White, 1997).

Imaging sub-basalt structures is notoriously complicated and there are several reasons why few successful case histories exist. The basalt flows are characterised by rough boundary topography and finely-layered internal structure. Therefore, scattering and attenuation are probably significant. Additionally, basalt can be considerably higher in velocity than the surrounding sediments. Hence, the point of critical *P*-wave reflection is reached at small incidence angle and only a small amount of *P*-wave energy penetrates the basalt layer. Finally, short-offset data is contaminated with multiples, again due to the high-impedance contrast with surrounding sediments.

The Rockall Trough which lies in deep-water west of Northern Ireland is the site of extensive intrusive and extrusive dolerites and basalts. Seismic exploration in this area presents both acquisition and processing challenges. We present a methodology for processing long-offset data recently acquired in this region. Our technique builds on the approach of Emsley et al. (1998) who use locally *P*-to-*S* converted waves recorded at far offsets to penetrate the basalt. The use of local mode conversions extends the range of useful offsets for imaging beneath interfaces with large velocity contrasts (Tatham et al., 1983; Tatham and Goolsbee, 1984). We improve upon the approach of Emsley et al. (1998) by also employing the τ-p transform to further isolate converted waves from multiples and head-waves and to increase the signal-to-noise ratio of the extracted waves. In addition, the τ-p transform enables us to isolate arrivals with specific incidence angles, thereby facilitating the distinction between converted-wave and pure-mode energy even further (Tatham et al., 1983; Tatham and Goolsbee, 1984).

Dataset

The dataset used in this study consists of long-offset streamer data acquired in the northern region of the Rockall Trough (west of Ireland). We present results of a 2D line which is roughly 35 km long with a 12.5 m CMP spacing. Each CMP gather is comprised of 180 traces with a trace interval of 50 m, totalling 9.2 km in maximum offset (first receiver-source distance is 250 m). Emsley et al. (1998) presented results for data acquired along a line which is nearly parallel to the line we analyse.

We focus on a 5 km subset of the line where the water depth is 1.1 km on average. One problem with the use of locally converted waves is that long offsets are required to record appreciable *P*-to-*S* conversions. The required streamer length depends critically on the depth of the top-basalt layer. In the part of the data considered, the basalt is some 600 m below the sea bottom (i.e., at 1.8 km depth) and 9 km offsets are adequate. However, in the part of the entire dataset which is over ultra-deep water (2.2 km), the top basalt is at 1.2 km below the sea floor (3.4 km depth). Here, 9 km offsets are insufficient.

Mode conversions and corridor mutes

Local mode conversion

Due to the large impedance contrast between the basalt and the overlying sediments, the point of critical *P*-wave reflection occurs at small incidence angles. Hence, only *P*-wave energy at near-incidence (i.e., short offsets) penetrates the basalt. Unfortunately, these *P*-wave sub-basalt reflections are of much smaller amplitude than the multiples related to the seafloor and top of basalt. As a consequence, multiple elimination often tends to also remove the desired sub-basalt primaries.

However, due to the large *P*-wave velocity contrast, *P*-to-*S* wave conversion is significant - especially if the *P*-wave velocity in the sediments is close to the *S*-wave velocity in the basalt (White and Stephen, 1980). Both phenomena are illustrated in Figure 1 for a *P*-wave incident on a high-velocity layer. Losses due to geometrical spreading are not incorporated in this figure. Since *P*-to-*S* conversion is so effective at the sediment-basalt interface, two locally converted waves

[1] *School of Earth Sciences, University of Leeds, Leeds, LS2 9JT, UK. E-mail: mvdbaan@earth.leeds.ac.uk*
[2] *Now at: Veritas DGC Ltd., Crompton Way, Manor Royal Estate, Crawley, RH10 2QR, UK. Previously: School of Earth Sciences, University of Leeds, Leeds, LS2 9JT, UK.*
[3] *School of Earth Sciences, University of Leeds, Leeds, LS2 9JT, UK. E-mail: kendall@earth.leeds.ac.uk*
[4] *Fugro-Geoteam AS, Hargreaves Road, Swindon, SN25 5AL, UK. E-mail: n.taylor@fugro.geoteam.no*

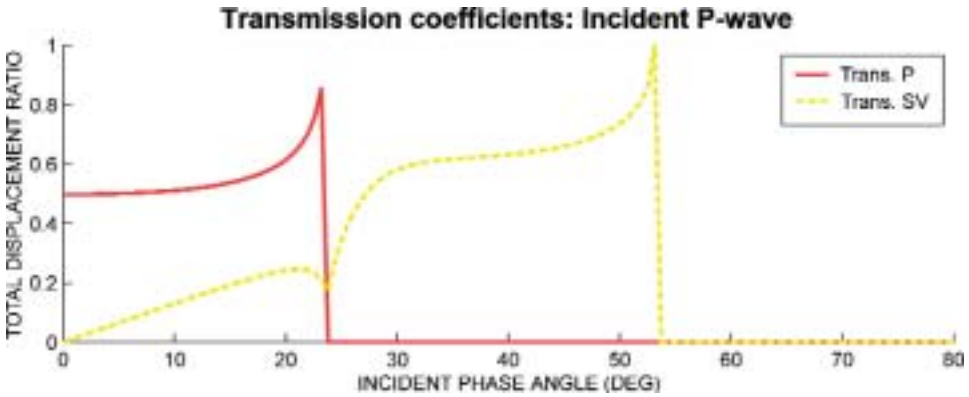

Figure 1 *Transmission coefficients for an incident P-wave on a sediment-basalt interface. Note that the point of critical P-wave reflection is quickly reached at an incidence angle of 24^0. P-to-S wave conversion is most significant between the points of critical P- and S-wave reflections. Post-critical transmission coefficients are not shown since associated arrivals are related to inhomogeneous waves that damp away exponentially with depth. Solid red line: P-wave transmission; dotted yellow line: S-wave transmission. Upper medium: v_P = 2 km/s, v_S = 1 km/s, ρ = 2.4 g cm-3; lower medium: vp = 5 km/s, vs = 2.5 km/s, ρ = 2.9 g cm-3.*

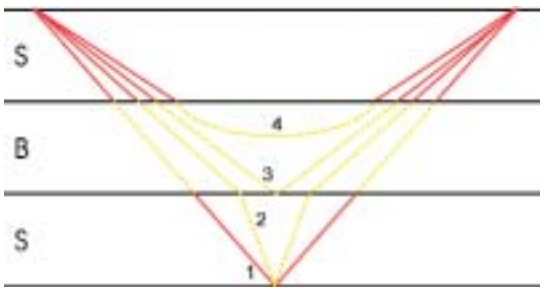

Figure 2 *Four different waves used in this study. 1 = PSP - PSP; 2 = PSS - SSP; 3 = PS - SP; 4 = diving PSP-wave. The top and bottom layer represent sediments, and the middle layer basalt. For the first three waves, the P-wave velocity of the sediments equals the S-wave velocity of the basalt layer and no vertical velocity gradients are present. Hence, the raypaths are straight lines. For the fourth wave, a strong vertical velocity gradient in the basalt layer is combined with a negative velocity jump between the upper P-wave sedimental velocity and the S-wave velocity of the basalt layer at the sediment-basalt interface. Note that in the latter case also the other three modes would show ray bending. Solid red line: P-waves; dotted yellow line: S-waves.*

can image sub-basalt structures - namely *PSS-SSP* and *PSP-PSP* waves. The first, second and third letter in this notation denote the type of wave above, within, and underneath the basalt for the down-going wave. The remaining letters are in reversed order and associated with the up-going wave upon reflection (Figure 2). Thus, the *PSS-SSP* wave is a double-converted wave where a downgoing *P*-wave converts to *S*-wave energy at the top of basalt, reflects as an *S*-wave and reconverts back to an *P*-wave again at the top of basalt. The *PSP-PSP*-wave undergoes 4 conversions at both the top and bottom of the basalt and reflects as a *P*-wave. It should also be noted that, although mode conversion at the sediment-basalt interface itself is efficient, the amplitude of the two converted arrivals are weak (due to geometrical spreading and transmission losses). They may even be weaker than the pure-mode *P*-waves penetrating the basalt layer. On the other hand, it will be shown below that they arrive in an offset-time window which is devoid of any other arrivals. They can therefore be detected as long as they exceed the background-noise level.

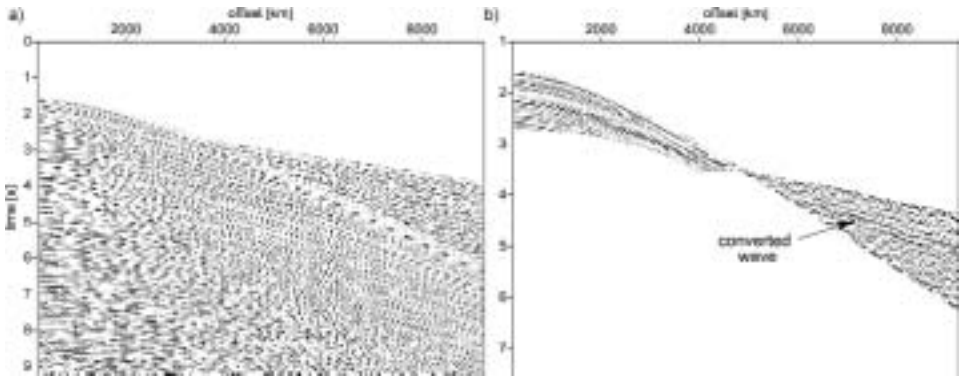

Figure 3 *x-t corridor-mute approach. (a) Raw CMP gather after bandpass filtering, AGC and top mute. (b) Time zoom-in on the CMP gather after application of the x-t corridor-mute technique (Emsley et al., 1998). Only the short-offset P-wave arrivals above the top-basalt reflection (2.2 s) and the converted waves between the top-basalt refraction and water-bottom reflection are conserved. A converted wave arrives between 7000 m at 4.3 s and 9200 m at 5 s.*

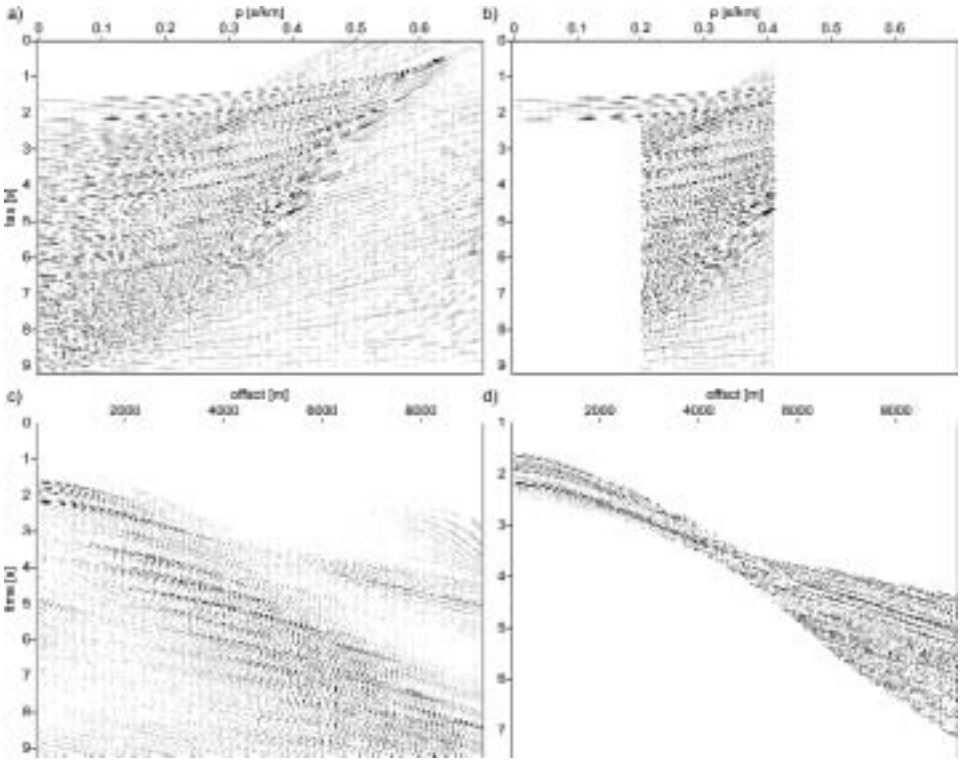

Figure 4 *τ-p corridor-mute approach. (a) τ-p transform of the CMP gather displayed in Figure 3a. The converted waves are clearly visible around p = 0.3 s/km and τ = 2.4 s. (b) τ-p mute window. This mute is devised such that the short-offset P-wave arrivals are conserved in addition to the converted waves in the far offset. Hence, all energy is muted for τ > 2.2 s and p < 0.2 s/km and for p > 0.4 s/km. (c) Resulting x-t gather after an inverse τ-p transform of Figure 4b. All short-offset multiples below the top-basalt reflection have been removed in addition to the far-offset water-bottom reflection. (d) Time zoom-in on the CMP gather after application of an AGC and an x-t corridor mute. Note that the continuity of the employed converted waves has been significantly improved and that an extra 1 second of data is extracted (compare with Figure 3b).*

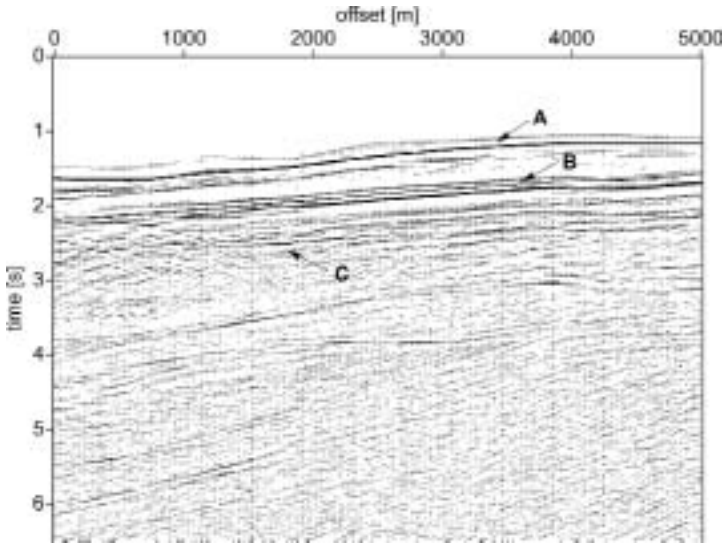

Figure 5 *Conventional stacked P-wave section over a 5 km distance. A: water bottom; B: top basalt. Deeper, dipping horizons are thought to be multiples with C the internal multiple between water bottom and top of basalt.*

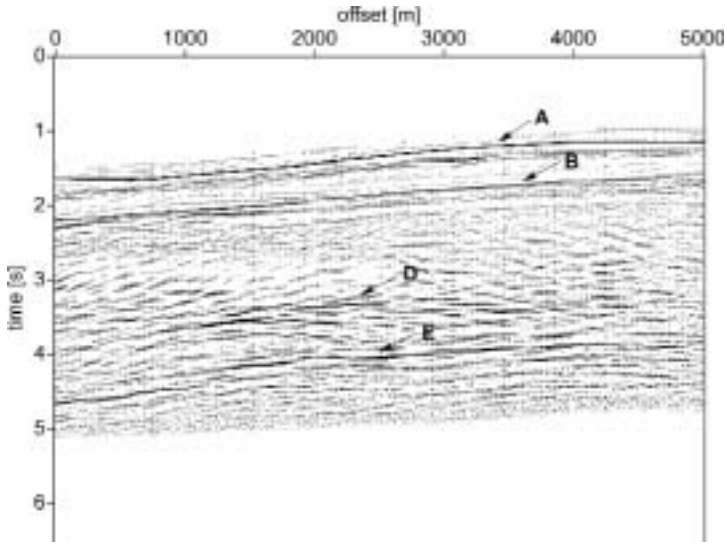

Figure 6 *Stacked section after x-t corridor mute. A: water bottom; B: top basalt; D + E may be sub-basalt reflections.*

Time-offset corridor mute

How can we detect such locally converted waves? Emsley et al. (1998) showed by means of raytracing in a simplified geological model that the *PSS-SSP/PSP-PSP* waves are most easily detected in a time-offset window in between the top-basalt refraction and the water-bottom reflection. Furthermore, multiple contamination is minimal in this far-offset window. They proposed therefore a very simple *x-t* corridor-mute approach to image sub-basalt structures.

A corridor mute similar to that proposed by Emsley et al. (1998) is shown in Figure 3. Only conventional short-offset *P*-wave data is employed to image reflections from above the top-basalt reflection. Later-arriving short-offset data is contaminated with multiples and therefore muted out. Sub-basalt structures are detected using the *PSS-SSP* and *PSP-PSP* waves arriving at times between the top-basalt refraction and the water-bottom *P*-wave reflection. All remaining far-offset energy is again muted out (Figure 3).

The advantage of this approach is that only waves with symmetrical raypaths are used and therefore these arrivals can be recorded and processed using conventional CMP methods. That is, they can be recorded using streamer lines and air guns, and CMP sorting and stacking is straightforward due to their symmetric raypaths. Furthermore, multiple contamination is minimal in this far-offset window. The stack velocities are estimated in the usual way after application of the corridor mute. In addition, any post-stack processing such as time migration remains possible once the stacked sections have been obtained.

The approach has the disadvantage that the converted waves only become noticeable at distances beyond the point of critical *P*-wave reflection at the top of the basalt. Hence, long-offset data need to be acquired. The minimum offset depends principally on the depth of the top basalt. In the Rockall area, 9 km seems to be adequate except over ultra-deep water (in excess of 2000 m).

τ-p corridor mute

We improve upon the technique of Emsley et al. (1998) by means of a τ-p transform. This particular transform relates traveltimes t and offsets x to intercept (delay) times τ and horizontal slownesses p (Diebold and Stoffa, 1981), and it has the specific advantage that it enables us to select seismic waves with particular incidence angles (Tatham et al., 1983; Tatham and Goolsbee, 1984). Snell's law implies that the horizontal slowness along a raypath is approximately constant in a medium that is more or less laterally homogeneous. This remains true even in the case of wave conversions. Since *P*-to-*S* conversion is most efficient for post-critical *P*-wave reflection, a selection on angle of incidence is advantageous. To put it differently, converted waves penetrating the basalt are characterised by larger horizontal slownesses than pure-mode *P*-wave signals and are therefore well separated in the τ-p domain.

The maximum slowness of pure-mode *P*-wave sub-basalt reflections is limited by the *P*-wave basalt velocity $v_{P,basalt}$ (say 5 km/s), whereas the horizontal slowness of *P*-waves converted to *S*-wave energy at the basalt top extends till the reciprocal of the *S*-wave basalt velocity $v_{S,basalt}$ (say 2.5 km/s). Furthermore, *P*-to-*S* conversion is most efficient for post-critical reflection, i.e. for $p > 1/v_{P,basalt}$. Thus, the slowness window that contains most *PSS-SSP* and *PSP-PSP* energy is for $1/v_{P,basalt} < p < 1/v_{S,basalt}$. The lower bound can easily be determined from the moveout of the top-basalt refraction. The upper bound, however, needs to be found by means of an educated guess unless well control is available or if the Poisson's ratio of the basalt is known.

We exploit the separation of signals in the slowness domain and apply a second corridor-mute technique in the τ-p domain. First, a top-mute is applied on the CMP gather just below the top-basalt refraction. The gathers are transformed to the τ-p domain (Figure 4a). The anti-alias filter of Moon et al. (1986) has been used in order to reduce the amount of aliasing. This filter screens the amplitudes of 3 adjacent traces along a slant line of particular slowness and only incorporates the central amplitude in the transform if the amplitude ratios are within predefined bounds. It also automatically reduces artifacts caused by the window edges.

The energy in the resulting τ-p gathers is then muted for all intercept times τ beyond the top-basalt *P*-wave reflection ($\tau > 2.2$ s) and $p < 1/v_{P,basalt}$ (Figure 4b). This removes all *P*-wave short-offset energy below the top-basalt reflection including most multiples. Furthermore, all energy for $p > 1/v_{S,basalt}$ is also muted to effectively remove all energy interfering with the converted waves at the far offsets (including, e.g., the water-bottom reflection). As a consequence, more converted-wave energy can be used for imaging.

An inverse τ-p transform is next applied to obtain a processed *x-t* gather (Figure 4c). The inverse transform uses again the anti-aliasing filter. Finally, the *x-t* corridor-mute technique of Emsley et al. (1998) is applied. The τ-p mute allows us to use a wider *x-t* mute window because contaminating energy is removed. This results in a significantly higher signal-to-noise ratio than the application of a single corridor-mute technique and an extra 1 second of converted-wave data becomes available due to the removal of the water-bottom reflection in the far offset (Figure 4d). Hence, deeper sub-basalt structures can be detected and, in principal, the minimum streamer length necessary for converted-wave processing can be reduced. The application of an *x-t* corridor mute also removes most of the remaining artifacts introduced by the forward and backward τ-p transforms such as the energy arriving around 3 s at the largest offsets.

Data application

The mixed-mode corridor-mute approach is tested on part of the dataset in the northern Rockall Trough. Figure 5 shows the conventional pure-mode *P*-wave stacked section. The water bottom (A) and top of basalt (B) are clearly visible. All deeper, dipping sub-basalt structures are thought to be multiples. For instance, the reflection (C) is most likely the inter-

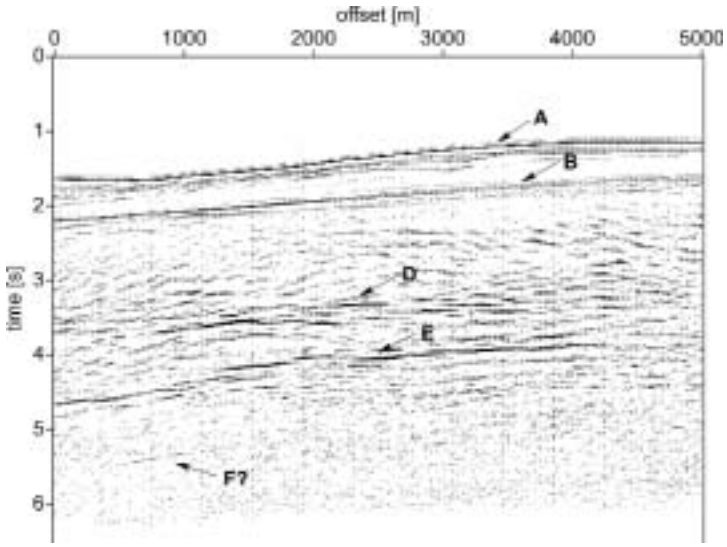

Figure 7 *Stacked section after combined x-t and τ-p corridor mutes. A: water bottom; B: top basalt; D, E and F: sub-basalt reflections?*

nal multiple between water bottom and top of basalt.

Next, the *x-t* corridor mute was applied on all CMP gathers associated with the same part of the dataset. The resulting stacked section is displayed in Figure 6 and contains potential sub-basalt structures D and E not detected by the conventional *P*-wave stack. The reflector C has disappeared however due to a slightly tighter mute window. Destructive interference with converted-wave energy whilst stacking has also reduced its amplitude since some of the converted-wave and pure-mode *P-P*-wave energy has near-identical vertical traveltimes after moveout corrections. The severity of this effect depends on the exact shape of the *x-t* corridor mute and the picked stack velocities. Furthermore, although we are dealing with far-offset arrivals, only second-order moveout corrections are applied since the converted-wave energy has an approximate linear moveout. Third-order (non-hyperbolic) corrections do not result in a higher stack quality. As a matter of fact, even a second-order (hyperbolic) moveout correction requires careful tuning because of missing zero-offset arivals.

Finally, Figure 7 shows the results after application of combined *x-t* and *τ-p* corridor mutes. The quality of the converted-wave stacked sections in Figures 6 and 7 is comparable. We are not certain whether to attribute this to a complicated sub-basalt geology or to the difficulty in obtaining an adequate stack velocity model. Accurate picking of the zero-offset traveltimes associated with the moveout velocities is more cumbersome than usual since the near-offset-converted wave energy is missing. This resulted in a 'tooth-like' behaviour of the sub-basalt reflections. We overcame the latter problem by smoothing the velocity field and thereby the zero-offset times. Nonetheless, a further 1 second of data is visible which may contain an event (F) not determined by the technique of Emsley et al. (1998). In addition, the sub-basalt reflections D and E are slightly better defined.

Interpretation

A thorough examination of both the reflections and refractions on the gather shown in Figure 3 reveals the following structural picture. The water depth is at 1.2 km and the basalt is overlain with a 600 m thick sedimentary package with an average *P*-wave interval velocity of 1.85 km/s (t_0 = 2.2 s). The basalt *P*-wave refraction clearly consists of two separate branches with moveout velocities of 4.07 km/s (for offsets of 3.4 to 5.5 km) and 5.15 km/s (5.5 km to 9.25 km), respectively. The latter refraction is tangent to a weak but visible reflection with a zero-offset traveltime of 2.33 s. From this we deduce that the basalt is composed of at least two layers and that the upper part is approximately 250 to 300 m thick. The sediment-basalt layer must have a strong *P*-to-*S* conversion coefficient. This would suggest a v_p/v_s ratio for the upper basalt layer near two ($v_{p,sediment}$ = 1.85 km/s and $v_{s,basalt}$ = 2.03 km/s). Smaller ratios would decrease strength of conversion.

The converted wave indicated in Figure 3 and corresponding to reflector D in Figures 6 and 7 has an approximate NMO moveout velocity of 2.4 km/s. We estimate the average interval velocity between this reflector and the top of basalt to be approximately 3.4 km/s using the Dix equation. Note

however that Dix equation is strictly speaking only valid for offset/depth ratios less than one.

From this point on the interpretation becomes a bit more ambiguous. If reflector D corresponds to the *PS-SP* reflection from the bottom of the basalt layer then we can model this reflection using a second basalt layer with an *S*-wave velocity of 3.4 km/s and a thickness of 800 m (which would mean v_p/v_s = 1.5). The resulting reflection only has a weak amplitude because of the significant velocity contrast within the basalt. The interval basalt reflection itself has a strong amplitude (roughly 1/5 to 1/3 of the top basalt reflection for offsets in excess of 2.5 km) but overlaps quite closely with both the top basalt and water bottom reflection in the far offset and remains therefore undetected. In this interpretation the question is why the v_p/v_s ratio drops from two in the upper layer to 1.5 in the lower one? If on the other hand reflector D corresponds to a sub-basalt reflection then it is most likely a quadruply converted *PSP-PSP* wave in order to maintain an average velocity of 3.4 km/s. In the latter case, *S*-to-*P* conversion at the bottom basalt is again most effective for sub-basalt sedimentary *P*-wave velocities near 3.4 km/s. This second interpretation leads to thinner basalt layers but leaves the question open as to why no bottom basalt reflection is detected.

Discussion

The corridor-mute windows effectively remove any remaining sub-basalt *P*-wave reflections. We are therefore confident that the detected sub-basalt reflections are related to converted-wave energy. Some of the deep reflectors apparent in the pure-mode *P*-wave section (Figure 5) may be related to those seen in Figures 6 and 7, but it is very difficult to make such a comparison. The converted-wave reflections will have larger traveltimes than pure-mode *P*-wave events. Accurate knowledge of *P*- and *S*-wave velocities and of the exact nature of these waves (*PSS-SSP* or *PSP-PSP*) is required for a rigorous comparison. Even so, multiple contamination in the *P*-wave section will always make this difficult. Indeed, such issues are serious challenges in any converted-wave processing (Gaiser, 1996; Kendall and Pullishy, 2002).

As an alternative to the τ-p corridor mute, the converted-wave energy can also be extracted by means of dip-filtering in the f-k domain. However, the nearly linear *PSS-SSP* and *PSP-PSP* events map onto lines in the f-k domain, whereas they map onto points in the τ-p domain. The τ-p transform has a higher gain in focusing power and therefore potentially a larger improvement in signal-to-noise ratio after extraction. A further advantage of signal separation in the τ-p domain is that the technique can easily be combined with Radon demultiple techniques. Moreover, it is less evident how to apply the proposed τ-p corridor-mute approach in the f-k domain. Other potential methods for increasing the signal-to-noise ratio are, for instance, the recognition and reconstruction techniques described in Van der Baan and Paul (2000), spatial-prediction filtering (Hornbostel, 1991), and approaches based on local τ-p analyses (Harlan et al., 1984; Kong et al., 1985).

The method can also be combined with the use of low-frequency sources as advocated by Ziolkowski et al. (2001). This has two distinct advantages. Firstly, any heterogeneous medium becomes effectively homogeneous for propagation distances of the order of a seismic wavelength (Backus, 1962). The effect of heterogeneities and discontinuities within the package of basalt are reduced by lowering the source frequency, thereby reducing the attenuation due to scattering (Van der Baan, 2001). This leads therefore to an improvement in the signal-to-noise ratio in both the pure-mode and combined-mode stacked sections. Lowering the source frequency does not eliminate the problem that a large impedance contrast may exist at the sediment-basalt interface which causes critical reflections to occur at small incidence angles. However, it does reduce the effects of interface topography and multiple scattering within the basalt.

Secondly, the pure-mode and combined-mode stacked sections are complementary in nature since mutually exclusive mute windows are employed. That is, both stacked sections can be obtained independently and thereafter used to interpret any sub-basalt structures in the other section. The quality of both stacked sections should improve by lowering the source frequency, thereby facilitating such a comparison.

Finally, extensive numerical modelling has shown that some ambiguity exists about the exact nature of the extracted converted waves and in particular about the propagation mode underneath the basalt layer. Potential candidates include both *PSS-SSP* and *PSP-PSP*-waves. This ambiguity does not invalidate the extraction or imaging technique, but does pose problems if time-to-depth conversion is needed. Nevertheless, the mixed-mode stacking technique was able to detect sub-basalt structures which were not visible in a conventional *P*-wave stack.

Another arrival which may cause ambiguities in the interpretation of the combined-mode stacked section is a diving *PSP*-wave. This particular arrival converts twice at the top of basalt and turns (no reflection) as an *S*-wave within the basalt layer due to the presence of a vertical velocity gradient (Figure 2). Modelling results indicate that this arrival may be equally strong or up to several times stronger than any *PSS-SSP* or *PSP-PSP* mode or even the *PS-SP* wave (reflection at the bottom of basalt) because of shorter raypaths and the absence of reflection. It is most likely to occur for moderately strong to strong velocity gradients ($\Delta v_s/\Delta z \geq 0.30 s^{-1}$) within thick basalt packages and for a positive jump between the *P*-wave velocity in the overlying sediments and the *S*-wave velocity of the basalt. The required velocity gradient reduces with an increasing positive velocity jump. However, too large a jump has a negative effect on the *P*-to-*S* conversion coefficient and thereby the amplitudes of any locally converted waves. In most situations, the *PSP*-wave will only arrive at distances much larger than the first detectable *PS-SP* wave. Modelling results show that the *PSP*-arrival will only occur

at distances larger than the actual streamer length (9 km) within the Rockall area unless strong velocity gradients are present ($\Delta v_s/\Delta z \geq 0.30s^{-1}$). In our opinion, the existence of such strong velocity gradients within the basalt is quite unlikely, however, since it would require a vertical *P*-wave gradient of approximately twice as large to maintain a constant Poisson's ratio (i.e., $\Delta v_p/\Delta z \geq 0.60s^{-1}$).

Conclusions

Locally converted waves can be used to image sub-basalt structures. The converted waves can be conveniently isolated in the far-offset domain in a region between the top-basalt refraction and the water-bottom reflection. A seismic image can be obtained using a mixture of pure-mode *P*-waves arriving at near offsets and converted-wave arrivals at far offsets. Above the top of basalt only conventional pure-mode *P*-waves are used, whereas any sub-basalt structures are detected using waves converted twice at the top of basalt. Such a mixed-mode imaging approach can conveniently be implemented using the *x-t* corridor-mute technique of Emsley et al. (1998). We improve upon their technique by means of an additional separation of signals using a τ-*p* mute.

A combined *x-t* and τ-*p* corridor mute yields a significantly higher signal-to-noise ratio in the CMP gathers than the application of a single mute technique. The continuity of the converted waves has been improved and an extra 1 second of data becomes available for imaging due to the removal of the far-offset water-bottom reflection. Sub-basalt structures in the final stacked section are also better defined.

This mixed-mode stacking technique is attractive as it relies on waves with symmetric raypaths only that can be recorded and processed using conventional CMP methods. That is, they can be recorded using streamer acquisition, and CMP sorting and stacking (migration) is straightforward. Furthermore, multiple contamination is minimal in this far-offset window. The disadvantage is that the converted waves only become noticeable at distances beyond the point of critical *P*-wave reflection at the top of the basalt. Hence, long-offset data need to be acquired. The minimum offset depends principally on the depth of the top of basalt. Nevertheless, the application of the mixed-mode corridor mutes to a dataset from the northern Rockall Trough reveals weak but coherent sub-basalt reflectors. In contrast the conventional *P*-wave section is dominated by multiples.

Acknowledgements

T. K. wishes to thank NERC for sponsoring his M.Sc. We are also grateful to Agip (a member of the ENI group) and Phillips Petroleum UK for permission to use this dataset. Financial support of Fugro-Geoteam is gratefully acknowledged. Finally, we thank Duncan Emsley and Pat Boswell for detailed information about their approach and Paul Williamson who suggested the diving *PSP*-wave as an alternative explanation.

References

Backus, G.E. [1962] Long-wave elastic anisotropy produced by horizontal layering. *Journal of Geophysical Research* **67**, 4427-4440.

Barton, A.J., and White, R.S. [1997] Crustal structure of the Edoras Bank continental margin and mantle thermal anomalies beneath the North Atlantic. *Journal of Geophysical Research* **102**, 3109-3129.

Diebold, J.B. and Stoffa, P.L. [1981] The traveltime equation, tau- mapping, and inversion of common midpoint data. *Geophysics* **46**, 238-254.

Emsley, D.B., Boswell, P.M., and Davis, P.G. [1998] Sub-basalt imaging using long offset reflection seismic data. *60th Meeting, European Association of Geoscientists and Engineers,* 1-48.

Gaiser, J.E. [1996] Multicomponent v_p/v_s correlation analysis. *Geophysics* **61**, 1137-1149.

Harlan, W.S., Claerbout, J.F., and Rocca, F. [1984] Signal/noise separation and velocity estimation. *Geophysics* **49**, 1869-1880.

Hornbostel, S. [1991] Spatial prediction filtering in the *t-x* and *f-x* domains. *Geophysics* **56**, 2019-2026.

Kendall, R.R., and Pullishy, J. [2002] A proposed workflow for converted-wave event registration - the step between processing and interpretation: *64th Meeting, European Association of Geoscientists and Engineers, P004.*

Kong, S.M., Phinney, R.A., and Roy-Chowdhury, K. [1985] A nonlinear signal detector for enhancement of noisy seismic record sections. *Geophysics* **50**, 539-550.

Moon, W., Carswell, A., Tang, R., and Dilliston, C. [1986] Radon transform wave-field separation for vertical seismic profiling data. *Geophysics* **51**, 940-947.

Tatham, R.H. and Goolsbee, D.V. [1984] Separation of *S*-wave and *P*-wave reflections offshore western Florida. *Geophysics* **49**, 493-508.

Tatham, R.H., Goolsbee, D.V., Massell, W.F., and Nelson, H.R. [1983] Seismic shear-wave observations in a physical model experiment: *Geophysics* **48**, 688-701.

Van der Baan, M. and Paul, A. [2000] Recognition and reconstruction of coherent energy with application to deep seismic reflection data. *Geophysics* **65**, 656-667.

Van der Baan, M. [2001] Acoustic wave propagation in one-dimensional random media: The wave localization approach. *Geophysical Journal International* **145**, 631-646.

White, R.S., and Stephen, R.A. [1980] Compressional to shear wave conversion in oceanic crust. *Geophysical Journal of the Royal Astronomical Society* **63**, 547-565.

Ziolkowski, A., Hanssen, P., Gatliff, R., Li, X., and Jakubowicz, H. [2001] The use of low frequencies for sub-basalt imaging. *71st Meeting, Society of Exploration Geophysics,* 74-77.